NONLINEAR QUANTUM WELL PHOTODETECTORS USING FREQUENCY UPCONVERSION

A Thesis

by

VENKATA RAMALAXMI CHAGANTI

Submitted to the Office of Graduate Studies of
Texas A&M University
in partial fulfillment of the requirements for the degree of

MASTER OF SCIENCE

December 2008

Major Subject: Physics

NONLINEAR QUANTUM WELL PHOTODETECTORS USING FREQUENCY UPCONVERSION

A Thesis

by

VENKATA RAMALAXMI CHAGANTI

Submitted to the Office of Graduate Studies of
Texas A&M University
in partial fulfillment of the requirements for the degree of

MASTER OF SCIENCE

Approved by:

Chair of Committee,	Alexey Belyanin
Committee Members,	Joseph H. Ross, Jr
	Christi Madsen
Head of Department,	Edward Fry

December 2008

Major Subject: Physics

ABSTRACT

Nonlinear Quantum Well Photodetectors
Using Frequency Upconversion. (December 2008)
Venkata Ramalaxmi Chaganti, B.S., Sri Sathya Sai University;
M.S., University of Hyderabad
Chair of Advisory Committee: Dr. Alexey Belyanin

I describe mid/far-infrared photodetectors based on frequency up-conversion in a near-resonant cascade of interband and intersubband transitions in high optical nonlinearity asymmetric quantum well structures. Such structures can yield high detectivity and responsivity in the mid/far-infrared range. Resonant up-conversion detectors can be designed for both collinear and perpendicular pump and signal beams. They can be integrated with semiconductor pump lasers to yield compact devices. Single photon counting is also achieved by these detectors. I present specific device designs based on GaAs/AlGaAs and InGaAs/AlInAs heterostructures and calculations of their expected figures of merit. This includes a study of the intersubband nonlinear absorption of asymmetric double quantum wells designed for mid/far-IR range. The dependance of second order nonlinear susceptibility on various parameters of the structure is studied. In particular, different values for barrier and well widths are considered. The nonlinear absorption can be obtained by using perturbative calculation of the linear susceptibility up to second order with density matrix approach. The intersubband linear and nonlinear asymmetric double quantum well can be tuned using two design parameters. One is the width of the barrier between the wells that controls the coupling and the second is the width of the narrow well that controls the asymmetry of the structure. As the barrier width narrows the en-

ergy gap at the anticrossing increases. The asymmetry of the two well potentials is essential for sum frequency and difference frequency generation since in a symmetric well $\langle Z_{31} \rangle = 0$ due to the same parity of the ground and second excited states so that $\chi^{(2)} = 0$. In our detection scheme using frequency up-conversion we demonstrate that these devices can achieve high detectivity, very low noise and high value for $\chi^{(2)}$ hence good efficiency. This can be an important advantage for low signal detection and single photon counting.

To My Family

ACKNOWLEDGMENTS

I wish to express my sincere gratitude to my advisor, Dr. Alexey Belyanin, for his help and support during the course of this reseach project. He was also very helpful in the editing of the manuscript.

I also would like to express my gratitude to Dr. Ross for helping me in the editing of this manuscript.

I also wish to thank Sergio Y. Rodriguez for helping me with Mathematica.

Finally I would to like to thank my family for their help and support.

TABLE OF CONTENTS

LIST OF FIGURES

FIGURE Page

CHAPTER I

INTRODUCTION

Sensors are used to detect optical radiation. They are generally categorized into two types, which are thermal detectors and photon detectors. In photon detectors the radiation is absorbed within the material by interaction with electrons that are either bound to lattice or impurity atoms. The electrical output signal results from the charged electronic energy distribution. The interaction generates free-charge carriers in intrinsic or extrinsic detectors [1], or delivers the necessary energy to charge carriers confined within a potential well to overcome the barrier.

Photon detectors exhibit a selective wavelength dependence of response per unit of incident radiation power. They exhibit good signal-to-noise performance and a very fast response, but to achieve this at mid/far-infrared wavelengths cryogenic cooling is needed. In mercury cadmium telluride detectors photo detection takes place due to interband transitions. Quantum well infrared photodetectors (QWIPs) are based on bound to bound intersubband transitions in quantum wells [2]. The transition energy determined by the energy levels in each quantum well can be varied by changing its structure. A good example is the structure made of GaAs/AlGaAs material [3]. The optoelectronic properties of a QWIP [4] can be designed by varying its structural parameters. By adjusting the Al fraction x, in the GaAs/AlGaAs system and the thickness of the GaAs layer at the time of growth, we can create a quantum well with optical properties tailored to a user's specifications.

This thesis follows the style of Journal of Applied Physics.

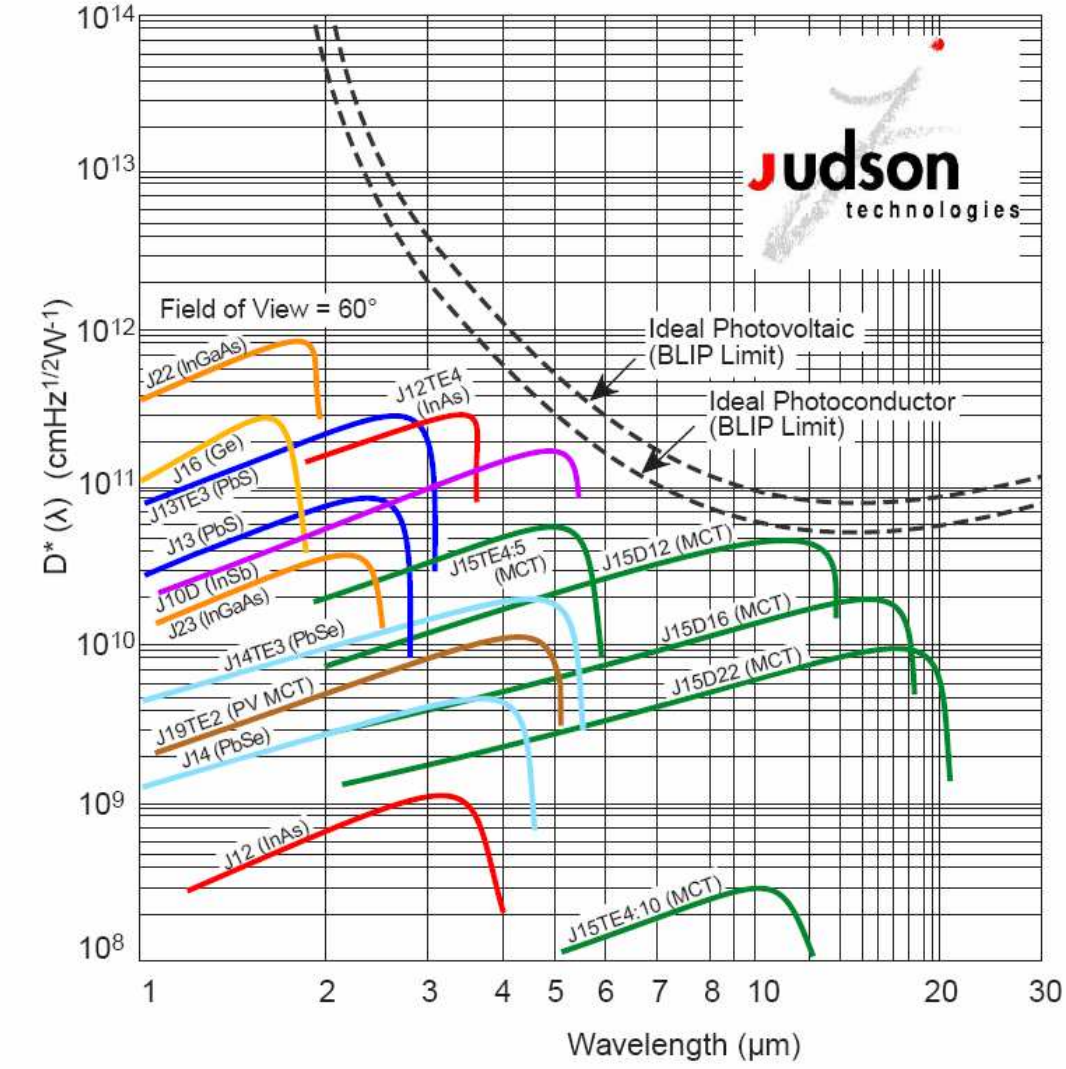

Fig. 1. State-of-the-art commercial photodetectors. Detectors with detectivity approaching the BLIP (Background Limited Infrared Performance) limit are liquid nitrogen cooled. From Judson Technologies.

Independently of their design, standard mid (3 to 25-40 microns)/far (greater than 40 microns)-infrared semiconductor photo detectors suffer from high dark currents due to thermal excitations across a low energy interband, intersubband or impurity transition. Cryogenic cooling is usually required for high detectivity. In general detectivity can be defined as

$$D^* = \frac{\sqrt{A\Delta\nu}}{NEP} \tag{1.1}$$

Where A is the surface area of the sample, $\Delta\nu$ is the band width and NEP is noise equivalent power, i.e the power at the detection limit corresponding to a signal-to-noise ratio of 1.

Fig. 1 shows that mid infrared detectors have low detectivity when compared to near infrared detectors at room temperature (Judson Technologies: http://www.judson technologies.com) To achieve high detectivity cryogenic cooling is needed. The detectivity is limited due to exponentially growing background blackbody radiation with increase in the wavelength even at BLIP (background limited infrared performance) conditions.

An alternative detection scheme is based on frequency up-conversion into the near-infrared (0.7-2 microns) or visible range. This approach allows one to use superior visible/near-infrared detectors such as avalanche photo diodes(APDs) and photo multipliers that have low dark currents and background noise and operate at room temperature in single photon counting regime. Mid/far-infrared detectors using frequency up-conversion give high detectivity but low quantum efficiency [5], which is the ratio between the flux of created carriers and the flux of incident photons.

In order to improve the efficiency, $\chi^{(2)}$ (second order nonlinear susceptibility) should be high. Recently efficient up-conversion from telecom wavelengths (1.3-1.55 μm) into the operating range of silicon avalanche photodiodes has been achieved [6, 7].

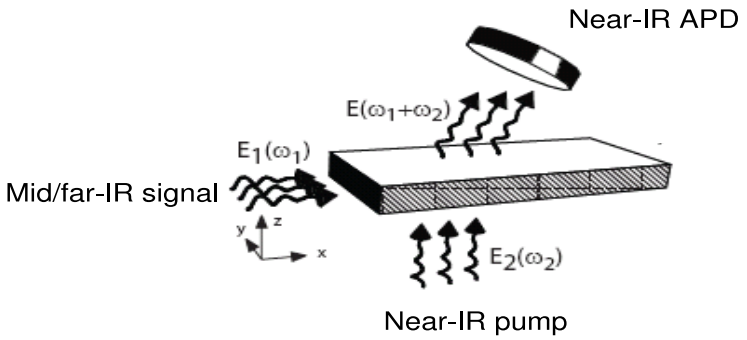

Fig. 2. A sketch of the up-conversion photodetection with orthogonal pump and input signal beams.

Mid-infrared single-photon counting using frequency up-conversion in a periodically poled lithium niobate crystal has been reported in [5]. Unfortunately, the efficiency of nonlinear up-conversion of weak signals is low, especially in the continuous-wave regime. For example, the up-conversion efficiency reported in [5] was of the order of 10^{-6}. It can be improved by employing high-power pulsed pump lasers, but the resulting system becomes bulky and inconvenient. It is known that the optical nonlinearity becomes strongly enhanced in resonant cascade schemes when all interacting fields are resonant with corresponding optical transitions in a medium. All practical up-conversion detector designs that could be potentially integrated with a pump source and other optoelectronic components require the use of solid-state nonlinear materials, preferably semiconductors. The crossed beam geometry in Fig. 2 is particularly interesting as it guarantees automatic phase matching and the up-converted signal propagates into a different direction than the pump laser beam [8]. In this thesis I examine and theoretically analyze various detection schemes of mid/far-infrared radiation by frequency up-conversion into the near-infrared range through resonantly enhanced sum-frequency generation in coupled semiconductor quantum well struc-

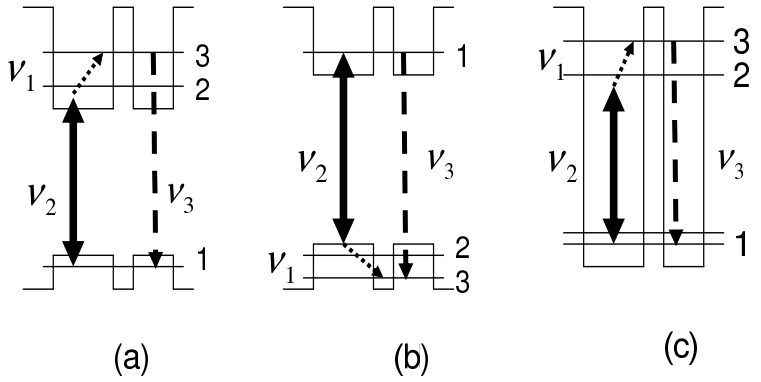

Fig. 3. A sketch of near-resonant SFG employing a cascade of interband and intersubband transitions (a, b) or intersubband transitions only (c). Bold solid line: a near-IR pump laser at frequency ν_2, dotted line: a mid/far-infrared signal at frequency ν_1, dashed line: an up-converted radiation at frequency $\nu_3 = \nu_1 + \nu_2$.

tures. The schemes utilize a near-resonant cascade of interband and intersubband transitions. A near-infrared laser pump, slightly detuned from the interband transition, is mixed with a mid/far-infrared signal resonant to the intersubband transition in the same structure, generating near-infrared sum-frequency radiation. A generic scheme of such process is shown in Fig. 3(a,b). In Fig. 3c we also sketch a variant of the SFG process utilizing only intersubband transitions in high band-offset heterostructures.

CHAPTER II

INTERBAND AND INTERSUBBAND TRANSITIONS IN QUANTUM WELLS

Intersubband transitions in quantum wells are the basis for QWIPs and for our frequency up-conversion scheme. Intersubband transitions lead to resonant absorption spectra for photons with energies equal to the energy spacing between nearly parallel subbands. QWIPs using the electron intersubband transitions usually employ grating couplers to couple thermal incident infrared radiation since the normal incident absorption is forbidden according to selection rules. Light is emitted or absorbed only when it is polarized in the growth direction. The strong Z direction confinement makes the electrons oscillate in the Z direction much faster than in X and Y directions. This confinement creates dipoles oriented along the Z direction which can radiate and absorb radiation only when polarized along Z. Quantum mechanically the intersubband transition rate between initial and final states can be calculated using Fermi golden rule,

$$W = |\langle \psi_f | H | \Psi_i \rangle|^2 (2\pi/\hbar) \delta(E_f - E_i - \hbar\nu) \tag{2.1}$$

where H is the dipole matrix Hamiltonian,

$$H = -\frac{e}{m_e c} Ap \tag{2.2}$$

Where A is the vector potential and p is the momentum operator. In general the matrix element of the momentum operator can be written as

$$\sum_{j=1}^{8} \langle \phi_{nj} | p_z | \phi_{n'j'} \rangle \langle u_j | u_{j'} \rangle + \sum_{j=1}^{8} \langle \phi_{nj} | \phi_{n'j'} \rangle \langle u_j | p_z | u_{j'} \rangle \tag{2.3}$$

where we have separated the wave functions into Bloch function (u) and envelope function (ϕ) components. The indices n, j, $n^{'}, j^{'}$ represent initial conduction band

states and final unoccupied valence band states respectively. The first term describes intersubband transitions and second term describes interband transitions. Interband transitions lead to staircase-like absorption spectra, with each step corresponding to the transition threshold of a paired electron subband and hole subband [9]. On the other hand intersubband transitions lead to resonant absorption spectra for photons with energies equal to the energy spacing between parallel subbands. Intersubband and interband transitions differ in parity selection rules for a symmetric well. For interband transitions, the transitions between the envelope functions of the same parity are stronger. In case of intersubband transitions, the transitions between the envelope functions of different parity are stronger, i.e transitions from odd to even states are allowed. In the case of asymmetric quantum wells all the transitions are dipole allowed. We considered electron intersubband and interband transitions in the GaAs/AlGaAs system as a function of QW thickness and aluminum concentration and barrier width.

CHAPTER III

NONLINEAR OPTICAL PROCESSES IN QUANTUM WELLS

Nonlinear-optical properties of quantum wells and super-lattices have become an object of intense study [10]. Nonlinear optics is the study of phenomena in which the optical properties of a material system get modified in the presence of light. In the case of linear optics, the induced polarization i.e the dipole moment per unit volume

$$\tilde{P}(t) = \chi^{(1)}\tilde{E}(t) \tag{3.1}$$

where the constant of proportionality $\chi^{(1)}$ is known as the linear susceptibility.

In the case of nonlinear optics, the optical response can often be described by expressing the polarization $\tilde{P}(t)$ as a power series in the field strength $\tilde{E}(t)$ as

$$\begin{aligned} \tilde{P}(t) &= \chi^{(1)}\tilde{E}^1(t) + \chi^{(2)}\tilde{E}^2(t) + \chi^{(3)}\tilde{E}^3(t) + \ldots, \\ &= \tilde{P}^{(1)}(t) + \tilde{P}^{(2)}(t) + \tilde{P}^{(3)}(t) + \ldots, \end{aligned} \tag{3.2}$$

here the quantities $\chi^{(2)}$, $\chi^{(3)}$, $\tilde{P}^{(2)}(t)$ and $\tilde{P}^{(3)}(t)$ are known as the second-order nonlinear susceptibility, third-order nonlinear susceptibility, second-order and third-order nonlinear polarizations respectively. The second-order nonlinear optical interactions can occur only in noncentrosymmetric systems.

The nonlinear optical properties can be explained in a more intutive way, in terms of an electron in a confining potential, is accelerated in this potential under an incident electromagnetic field. The accelerated electron oscillates and radiates according to its motion in the potential. The observed optical properties of the material rely on this motion. If the potential is asymmetric and the driving field is large enough to force the electron into the noticeably nonharmonic portion of the potential then the

reradiated light will contain higher harmonics. The actual shape of the potential determines the relative strength of the higher harmonics, leading to, for example, second harmonic generation (SHG) or third harmonic generation (THG). Similarly we can infer that an electron in any asymmetric potential driven by two different incident electric fields will radiate the sum-frequency/difference frequency of the two incident fields. This results in sum frequency generation (SFG)/difference frequency generation (DFG).

A. Nonlinear Optical Interactions

In this section, I present brief qualitative descriptions of second order nonlinear optical interactions. We consider the situation in which the optical field incident upon a nonlinear optical medium characterized by a nonlinear susceptibility $\chi^{(2)}$ consists of two distinct frequency components, as

$$\tilde{E}(t) = E_1 e^{-i\nu_1 t} + E_2 e^{-i\nu_2 t} \tag{3.3}$$

In the above equation we assume that the second-order contribution to the nonlinear polarization is of the form

$$\tilde{P}^{(2)}(t) = \chi^{(2)} \tilde{E}(t)\tilde{E}^{*}(t) \tag{3.4}$$

Hence, the nonlinear polarization is given by

$$\begin{aligned} \tilde{P}^{(2)}(t) = \chi^{(2)}[E_1^2 e^{-2i\nu_1 t} + E_2^2 e^{-2i\nu_2 t} + 2E_1 E_2 e^{-i(\nu_1+\nu_2)t} + \\ 2E_1 E_2^{*} e^{-i(\nu_1-\nu_2)t} + c.c] + 2\chi^{(2)}[E_1 E_1^{*} + E_2 E_2^{*}] \end{aligned} \tag{3.5}$$

We can also express this result as

$$\tilde{P}^{(2)}(t) = \sum_n P(\nu_n) e^{-i\nu_n t} \tag{3.6}$$

here the summation extends over positive and negative frequencies ν_n. The complex amplitudes of the various frequency components of the nonlinear polarization are hence given by

$$\begin{aligned} P(2\nu_1) &= \chi^{(2)} E_1^2, \\ P(2\nu_2) &= \chi^{(2)} E_2^2, \\ P(\nu_1 + \nu_2) &= 2\chi^{(2)} E_1 E_2, \\ P(\nu_1 - \nu_2) &= 2\chi^{(2)} E_1 E_2^*. \end{aligned} \tag{3.7}$$

In the above expression the first two terms represent second harmonic generation and the second and third terms represent sum frequency and difference frequency generations respectively. Among the four different nonzero frequency components present in the nonlinear polarization only one of these frequency components will be present with any appreciable intensity in the radiation generated by the nonlinear optical interaction. This is due to the fact that the nonlinear polarization can efficiently couple to an electromagnetic wave only if a certain phase-matching condition is satisfied. Which frequency component will be radiated depends also on the polarization of the input radiation and orientation of the material system.

Quantum confinement of carriers leads to the existence of strong resonances in the absorption spectra attributed to both interband and intersubband transitions. The existing theoretical and experimental studies of nonlinear optical properties of quantum wells can be divided into two groups: those examining photon energies in the infrared that are due to intersubband transitions and others dealing with energies

in the visible range that are due to interband transitions. In a symmetric quantum well, because of the same parity of the ground state and second excited state the corresponding dipole matrix element ($\langle Z_{31} \rangle$) is 0 so that $\chi^{(2)} = 0$. Hence we need to break the symmetry of the well; asymmetry of the two well potential is essential for sum frequency generation. In order to maximize $\chi^{(2)}$ in any system we need to maximize the product of dipole matrix elements. In the case of an asymmetric double quantum well, by designing its structure, we can achieve the maximum product of dipole moments. There exist many advantages of intersubband processes such as their large oscillator strengths, narrow line widths and large dipole matrix elements (10-20 $\mathring{A}$) [11]. Large second order nonlinearities based on intersubband resonant enhancement were first observed by Gurnick and De Temple in 1983 [12]. Early analytical expressions for all of the most important second-order nonlinear coefficients in asymmetric quantum well structures were deduced in 1989 [13]. Systematic theoretical and experimental analysis of resonant optical nonlinearities in quantum well semiconductor lasers has been reviewed in [14, 15] and mid-infrared quantum cascade laser sources based on intra-cavity nonlinear frequency conversion is discussed in [16, 17, 18]. Resonant QW schemes for the up-conversion detection of mid/far-infrared radiation were proposed and analyzed in [8, 19]. The discussion in the next chapter largely follows these references.

CHAPTER IV

NONLINEAR OPTICAL SUSCEPTIBILITY

In any medium, the nonlinear susceptibilities of order n, are in general sums of various contributions, each containing in the numerator the product of $(n+1)$ dipole matrix elements and in the denominator products of linear combinations involving the difference between photon frequencies participating in the nonlinear interaction and complex transition frequencies of the system. We consider the second order nonlinear susceptibility. To optimize $\chi^{(2)}$ in any quantum well we therefore need to maximize the product of dipole elements of transitions and to minimize energy denominators, using resonant effects. In this chapter we consider a three level system and show the necessary steps to obtain the nonlinear susceptibility.

Let us consider the hamiltonian of the form

$$H = H_0 + H_1 \tag{4.1}$$

where H_1 is the dipole interaction term $-qrE(t)$, in which q is the electron charge, r is the position operator in the direction parallel to the electric field $E(t)$.

The density matrix equation has the form

$$\dot{\rho}_{nm} = -\frac{i}{\hbar}[\hat{H}, \hat{\rho}]_{nm} - \gamma_{nm}\rho_{nm} \tag{4.2}$$

The elements of density matrix have the following physical interpretation. The diagonal elements ρ_{nn} give the probability that the system is in energy eigenstate n. The off-diagonal elements ρ_{nm} represent the coherence between levels n and m. For a three level system we can represent H_0 and H_1 in the following way.

$$H_0 = \hbar\omega_1|1\rangle\langle 1| + \hbar\omega_2|2\rangle\langle 2| + \hbar\omega_3|3\rangle\langle 3| \tag{4.3}$$

and

$$H_1 = -\hbar(\Omega_1^* e^{i\phi_1} e^{i\nu_1 t}|1\rangle\langle 2| + \Omega_2^* e^{i\phi_2} e^{i\nu_2 t}|2\rangle\langle 3| + \Omega_3^* e^{i\phi_3} e^{i\nu_3 t}|1\rangle\langle 3|) \tag{4.4}$$
$$-\hbar(\Omega_1 e^{-i\phi_1} e^{-i\nu_1 t}|2\rangle\langle 1| + \Omega_2 e^{-i\phi_2} e^{-i\nu_2 t}|3\rangle\langle 2| + \Omega_3 e^{-i\phi_3} e^{-i\nu_3 t}|3\rangle\langle 1|)$$

Here Ω is the complex Rabi frequency of the corresponding fields that can be written as

$$\Omega_{i,j,k} = \frac{\mu_{i,j,k} E(t)}{2\hbar} \tag{4.5}$$

and $\mu_{i,j,k}$ represent dipole moments of the corresponding transitions.

We consider second order susceptibility for the process of resonant sum-frequency generation in a three level system in which ν_1 and ν_2 are different and $\nu_3 = \nu_1 + \nu_2$ is the resultant signal (see Fig.4.).

In the rotating wave approximation, introducing slowly varying amplitudes of the off-diagonal elements of the density matrix

$$\rho_{ij} = \sigma_{ij} e^{-i\nu t}. \tag{4.6}$$

the density matrix equations for populations can be written as

$$\dot{\rho}_{11} = -2Im[\Omega_3^* \sigma_{31}] - 2Im[\Omega_1^* \sigma_{21}] + r_{12}\rho_{22} + r_{31}\rho_{33} \tag{4.7}$$

$$\dot{\rho}_{22} = -2Im[\Omega_2^* \sigma_{32}] + 2Im[\Omega_1^* \sigma_{21}] + r_{32}\rho_{33} - r_{21}\rho_{22} \tag{4.8}$$

$$\dot{\rho}_{33} = 2Im[\Omega_3^* \sigma_{31}] + 2Im[\Omega_2^* \sigma_{32}] - (r_{31} + r_{32})\rho_{22} \tag{4.9}$$

where r_{ik} are relaxation rates of transitions $i \longrightarrow k$.

The equations for amplitudes of the off diagonal matrix elements can be written

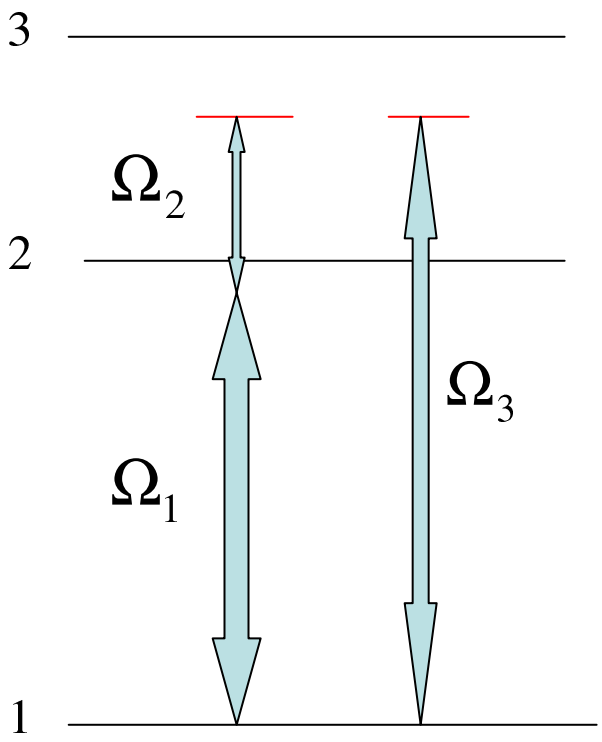

Fig. 4. Sketch of a three level system interacting with three fields with Rabi frequencies Ω_1, Ω_2 and Ω_3.

as

$$\dot{\sigma}_{21} + \Gamma_{21}\sigma_{21} = i\Omega_1 n_{12} + i\Omega_2^* \sigma_{31} - i\sigma_{32}^* \Omega_3 \tag{4.10}$$

$$\dot{\sigma}_{32} + \Gamma_{32}\sigma_{32} = i\Omega_2 n_{23} - i\Omega_1^* \sigma_{31} + i\sigma_{21}^* \Omega_3 \tag{4.11}$$

$$\dot{\sigma}_{31} + \Gamma_{31}\sigma_{31} = i\Omega_3 n_{13} - i\Omega_1 \sigma_{32} + i\sigma_{21}^* \Omega_2 \tag{4.12}$$

where $n_{ij} = \rho_{ii} - \rho_{jj}$,

$$\Gamma_{21} = \gamma_{21} + i(\omega_{21} - \nu_1) \tag{4.13}$$

$$\Gamma_{32} = \gamma_{32} + i(\omega_{32} - \nu_2) \tag{4.14}$$

$$\Gamma_{31} = \gamma_{31} + i(\omega_{31} - \nu_3) \tag{4.15}$$

Now we consider steady state

$$\dot{\sigma_{ij}} = 0. \tag{4.16}$$

In order to obtain the nonlinear susceptibility we solve for σ_{21}, σ_{32} and σ_{31}. The polarization at the sum frequency is proportional to σ_{31}.

By solving the above three equations at the steady state we can obtain σ_{21}, σ_{32} and σ_{31}. For sum frequency generation σ_{31} can be written as

$$\sigma_{31} = \frac{\Omega_1\Omega_2(\frac{n_{21}}{\Gamma_{21}} + \frac{n_{23}}{\Gamma_{32}}) + i\Omega_3(n_{13} + \frac{|\Omega_1|^2 n_{21}}{\Gamma_{21}^*\Gamma_{32}} - \frac{|\Omega_2|^2 n_{23}}{\Gamma_{21}\Gamma_{32}^*})}{\Gamma_{31} + \frac{|\Omega_1|^2}{\Gamma 32} + \frac{|\Omega_2|^2}{\Gamma 21}}. \tag{4.17}$$

In the above derivation we considered Ω_1 and Ω_2 be the strong fields and Ω_3 to be the weak field.

The second order nonlinear polarization, neglecting higher order terms in (4.18), is given by

$$P(\nu_1 + \nu_2) = \chi^{(2)}(\nu_1 + \nu_2)E_1(\nu_1)E_2(\nu_2). \tag{4.18}$$

The second-order nonlinear susceptibility for the process sum frequency can be written as

$$\chi^{(2)} = \frac{N}{\hbar^2}\frac{\langle\mu_{12}\rangle\langle\mu_{23}\rangle\langle\mu_{13}\rangle}{\Gamma_{31}}(\frac{n_{21}}{\Gamma_{21}} + \frac{n_{23}}{\Gamma_{32}}). \tag{4.19}$$

Where N is the electron density in the wells, ϵ_0 is the permitivity of the vacuum, q is the electron charge and $\langle\mu_{12}\rangle$, $\langle\mu_{23}\rangle$ and $\langle\mu_{31}\rangle$ are the transition matrix elements. The intersubband matrix elements are typically in the 10-20 $\mathring{A}$ range, leading to high oscillator strengths. The interband matrix elements are of the order of 1-5 $\mathring{A}$. The multiple resonance effects are responsible for the extremely large nonlinearities in the infrared. In case of interband transitions both the dipole moments, relaxation rates and energies of the corresponding transitions depend on $k_{||}$ (see Fig.5.) While calculating $\chi^{(2)}$ for interband transitions integration over $k_{||}$ is needed, where the absolute value of $k_{||}$ is defined as $\sqrt{k_x^2 + k_y^2}$ where (k_x, k_y) is a point in the quantum well plane.

For a given detuning, the strength of the nonlinearity is characterized by the product of the three dipole moments $\langle\mu_{12}\rangle\langle\mu_{23}\rangle\langle\mu_{31}\rangle$ where $\langle\mu_{ij}\rangle = q\langle Z_{ij}\rangle$. To obtain a large value of the product one needs to use asymmetric heterostructures. A vast number of different configurations has been proposed in the literature. We use an asymmetric double quantum well structure. We have performed k.p simulations

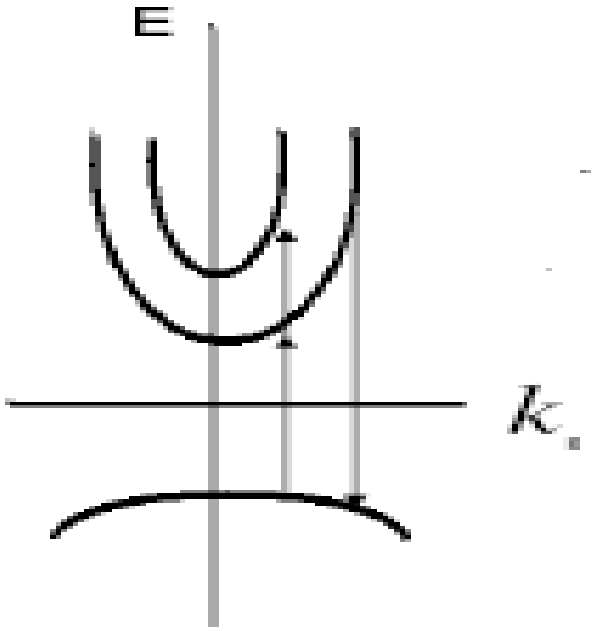

Fig. 5. Electron energy as a function of parallel momentum $k_{||}$.

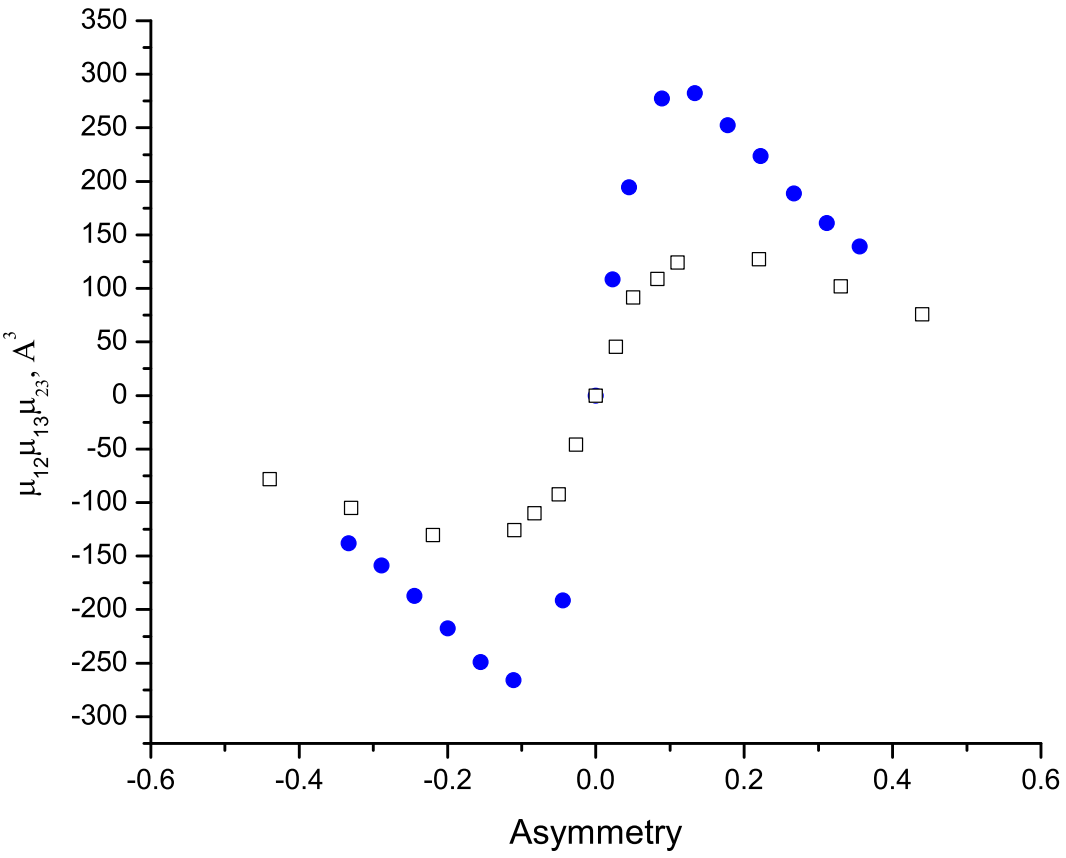

Fig. 6. The product of three dipole moments as a function of the normalized asymmetry of a double QW, defined as $\frac{d_1-d_3}{d_1+d_2+d_3}$, where $d_{1,3}$ are the thicknesses of two QWs and d_2 is the thickness of a barrier in between. Open squares represent InGaAs/AlInAs heterostructure lattice matched to InP and open circles represent GaAs/AlGaAs heterostructure. Graphs are plotted for a constant $(d_1 + d_2 + d_3) = 90\mathring{A}$ and $d_2 = 10\mathring{A}$.

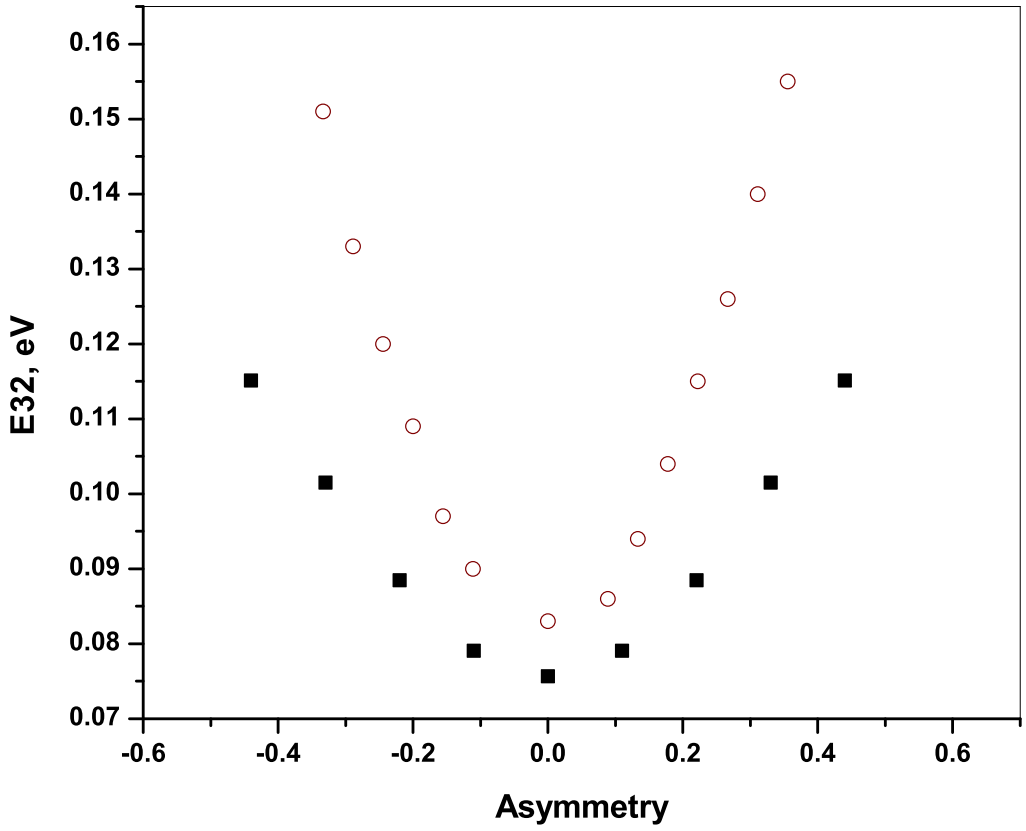

Fig. 7. The intersubband transition energy as a function of the normalized asymmetry of a double quantum well, defined as $\frac{d_1-d_3}{d_1+d_2+d_3}$, where $d_{1,3}$ are the thicknesses of two QWs and d_2 is the thickness of a barrier in between. Open circles represent InGaAs/AlInAs heterostructure lattice matched to InP and solid squares represent an GaAs/AlGaAs heterostructure. Graphs are plotted for a constant $d_1 + d_2 + d_3 = 90\mathring{A}$ and $d_2 = 10\mathring{A}$.

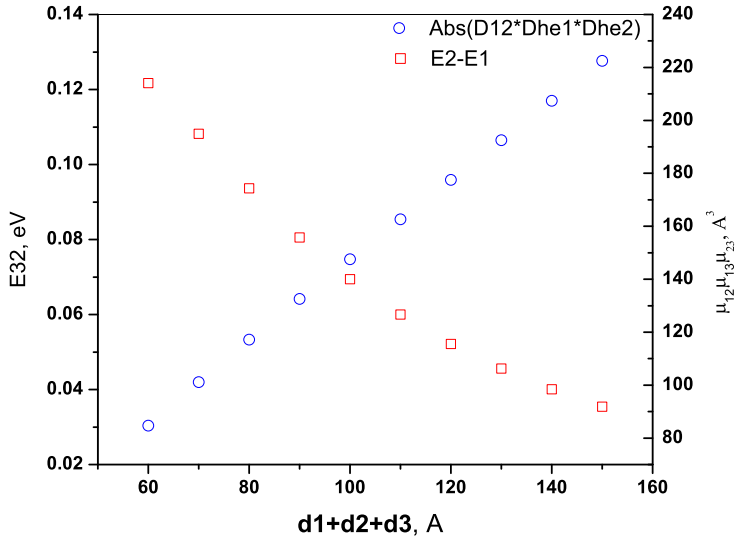

Fig. 8. The intersubband transition energy represented by the squares on left axis and the product of three dipole moments represented by circles on right axis as functions of the total thickness $d_1+d_2+d_3$ of a double GaAs/AlGaAs QW, where $d_{1,3}$ are the thicknesses of two QWs and d_2 is the thickness of a barrier in between. Graphs are plotted for a constant asymmetry ratio $(d_1-d_3)/(d_1+d_2+d_3) = 0.2$ and $d_2 = 10\mathring{A}$.

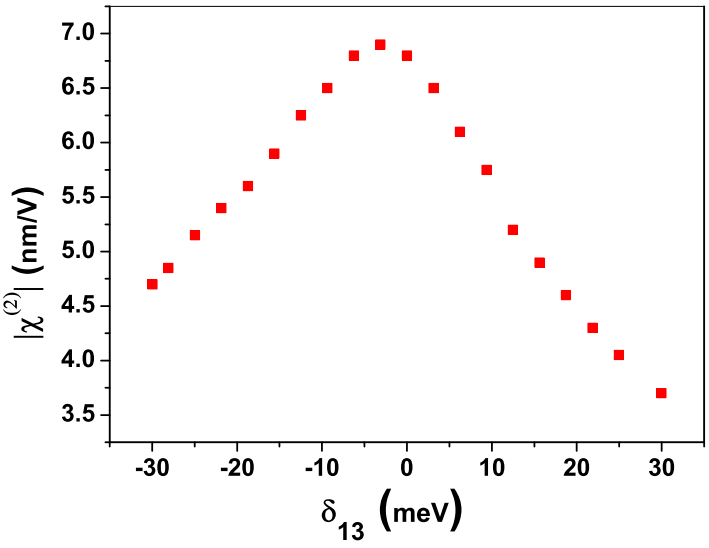

Fig. 9. The value of $|\chi^{(2)}|$ as a function of detuning of the up-converted signal frequency from the transition 1-3. All parameters are specified in the text.

in various approximations (from 8-band to effective 3-band) for a large number of QW configurations and found that for a given material system and given intersubband energy the maximum values of the above product are similar within a factor of 2. In Fig. 6-8 we show the simulation results for unbiased double QW for two heterostructures. One is the InGaAs/AlInAs heterostructure lattice matched to InP and the other is GaAs/AlGaAs heterostructure. These figures illustrate optimal QW thickness, asymmetry and maximum nonlinearity achieved in these heterostructures for various intersubband transition energies in the mid/far-infrared range. Peak responsivity of the detector is reached at the photon energy of the signal roughly equal to the intersubband transition energy. From figures 6-8 one can choose the optimal structure of the nonlinear system for a given wavelength.

Fig. 9 shows the value of $|\chi^{(2)}|$ as a function of detuning δ_{13}, when the pump laser is detuned by 20 meV below the absorption edge $E_{21}(0)$. All numerical values are

chosen for a double quantum well InGaAs/AlInAs heterostructure lattice matched to InP, with all line broadenings γ (half-widths at half maximum) equal to 10 meV and the product of three dipole moments equal to 280 A^3 (from Fig.6). The structure consists of 30 A and 22 A QWs separated by a 20 A barrier. As is clear from the figure, the full width at half-maximum of the spectral response of the detector is about 46 meV, i.e about 1/3 of the mid-infrared signal frequency (120 meV). Tuning pump laser closer to the band gap increases the maximum nonlinearity but also increases the pump absorption, which leads to enhanced spontaneous recombination of photoexcited electrons and ultimately to higher noise-equivalent power and lower detectivity. One should choose an optical pump detuning depending on the specific application.

The multiple resonance effects are responsible for the extremely large nonlinearities and the large value of $\chi^{(2)}$ in the infrared. Maximum values of $|\chi^{(2)}|$ in the mid-infrared range at 10μm wavelength are within 5-20 nm/V. The nonlinearity in the InGaAs/AlInAs heterostructure is stronger by a factor of 2-3 as compared to the GaAs/AlGaAs system. However, because of a narrower band gap of InGaAs the wavelengths of the up-converted signal are typically in the range 1.1-1.2 μm. For detection in this range one has to use InGaAs APDs that have lower efficiency compared to silicon APDs. In GaAs-based heterostructures the up-converted signal does fit into the operating range of superior silicon APDs.

A. Detector Geometry and Up-Conversion Efficiency

The detector geometry and beam alignment depend on which of the up-conversion schemes on Fig.3 one chooses. For a scheme on Fig.3a, the mid/far-infrared signal should have a TM-polarization and come from the facet, while the near-IR pump

can either come from the facet or propagate at normal incidence to the layers as shown in Fig.2. For a scheme in Fig.3b both signal and pump are allowed to have TE polarization and propagate normal to the layers if the transition 2-3 occurs between the first heavy-hole and second light-hole subbands. Normal incidence is an important advantage; however in this case maximum nonlinearity is lower by a factor of 7-8 as compared to using a TM-polarized intersubband transition. Finally for a scheme in Fig.3c all beams should have TM-polarization and therefore propagate parallel to the QW layers. For the geometry of Fig.2 the total output SFG power in the phase-matched direction is

$$P = \frac{2\pi N\omega^4}{c^3}\frac{|\chi^{(2)}|^2(A_1A_2)^2L_z^2L_x}{k_z^2}. \tag{4.20}$$

Where L_x is the length of the pumped spot in the x-direction, L_z is the active region thickness, A_1 and A_2 are the amplitudes of the electric fields of mid-infrared signal E_1 and near-infrared pump E_2 respectively. Assuming that the mid-infrared signal has overlap Γ with the active region in z-direction, and the pump and the signal are overlapped over the length L_y in y-direction, the above equation can be expressed through the total signal power P_1 and the pump intensity in the mixing region I_2 as

$$P = \frac{4\pi^3\omega^2}{c^3nn_1n_2}|\chi^{(2)}|^2L_zL_x\Gamma I_2P_1, \tag{4.21}$$

where n, n_1, n_2 are the refractive indices of three interacting beams in the active region. Note that the mid-IR radiation can be guided in the crystal in which case n_1 is an effective modal refractive index. The power up-conversion efficiency defined as $\eta_{up} = \frac{P}{P_1}$ is an important figure of merit of the detector.

B. Detector Performance

Although the proposed mid/far-infrared photodetection scheme consists of two steps i.e. up-conversion and subsequent detection by a near-IR APD, it can be still charecterized by standard figures of merit. They are the noise equvivalent power(NEP), which is inversely proportional to the detectivity, the quantum efficiency and the responsivity. The intrinsic noise of our detector in the absence of an input signal has several contributions: an intrinsic noise of the near-IR APD, background radiation at the sum frequency, background noise at the mid-IR signal frequency up-converted by SFG processes, and spontaneous recombination emission of the QW structure in the absence of a signal that gets intercepted by an APD. The detection sensitivity is a measure of the minimum signal level that can be detected. It indicates the amount of power, in watts, to obtain a signal-to-noise ratio of unity. In other words the signal to noise ratio can be written as

$$\frac{S}{N} = \frac{P_{inc}}{NEP}. \tag{4.22}$$

Here NEP is given by the expression

$$NEP = \frac{\hbar\omega_1}{\eta_{phot}}\langle n_{tot}\rangle, \tag{4.23}$$

where $\langle n_{tot}\rangle$ describes the detection noise statistics and η_{phot} is the total quantum efficiency. It comprises all statistically independent sources of noise, namely, dark counts n_{DC} (inherent in the Si APD), background noise n_{BG} and P_{sp} such that

$$\langle n_{tot}\rangle = \langle n_{DC}\rangle + \langle n_{BG}^{up}\rangle + \langle n_{BG}^{NIR}\rangle + P_{sp}. \tag{4.24}$$

η_{phot} is given by

$$\eta_{phot} = \eta_{up}\frac{\omega_1}{\omega_3}\eta_{NIR}, \tag{4.25}$$

where η_{up} is the power up-conversion efficiency which is the ratio power of the sum-frequency generated signal and the power of incident signal. η_{NIR} is the efficiency of the near-IR APD.

The background noise consists in all counts generated by external photons other than the signal photons. In our case we also have spontaneous recombination noise at the sum frequency coming from the quantum wells. Ideally we would like to have all contributions to be lower than or comparable to the intrinsic APD noise. In this case the detectivity of the whole scheme is determined by the detectivity of the near-IR APD. The up-converted back-ground noise is mostly filtered out by the phase-matched SFG process since only one spatial mode of this noise can be up-converted efficiently.

Spontaneous emission at frequencies near the sum frequency ν from the MQW structure is due to excitation of electrons and holes by a strong pump, followed by radiative recombination of a hot tail of the distributions of photoexcited carriers having parallel momenta $k_{||}$ satisfying the condition

$$E_{21}(k_{||}) \approx E_{21}(0) + \frac{\hbar^2 k_{||}^2}{2m_e} + \frac{\hbar^2 k_{||}^2}{2m_h}, \tag{4.26}$$

$$\hbar\nu = E_{21}(0) + \frac{\hbar^2 k_{||}^2}{2m_r}. \tag{4.27}$$

The noise signal power reaching the detector within the frequency bandwidth $\Delta\nu$ and a solid-angle aperture $\Delta\Omega \ll 1$ of the detector, which is set to receive only a highly collimated sum-frequency signal, can be estimated as

$$P_{sp} = A(k_{||})N_e(k_{||})V_{MQW}\Delta\nu\frac{\Delta\Omega}{4\pi}, \tag{4.28}$$

where A is the spectral density of the spontaneous emission rate and V_{MQW} is the pumped volume of the active region. The density of hot electrons and holes with a

given parallel momentum obeys Boltzmann distribution in the simplest case. It can be calculated from the absorbed power of the pump radiation and can be controlled by the detuning δ_{12} of the pump below the band edge and by the pump intensity I_2. Recent advances have pushed the NEP of APDs to very low values of 10^{-15} W $cm^{-1/2}$ even for the InGaAS APDs at room temperatures [20]. Ideally P_{sp} should be below the NEP of the near-IR APD, which limits the pump intensity I_2 to about 10^6 W/cm^2 for $E_{32} \sim 100$ meV, $\Delta\Omega \sim 0.01$, $\delta_{12} \sim 30$ meV, and resonable values for all other parameters. Another kind of noise specific to the up-conversion detection is due to the fact that the output sum-frequency signal is effectively modulated by the pump laser intensity. The pump laser can have intensity fluctuations, a kind of noise known as Relative Intensity Noise (RIN). This noise will introduce small fluctuations in the output power, proportional to the intensity of the signal. This noise can be neglected for NEP calculations, but it can introduce a certain noise level depending of the specific system. The overall photon conversion efficiency is given by

$$\eta = \frac{\omega_1}{\omega}\eta_{up}\eta_c\eta_{APD}, \tag{4.29}$$

where $\eta_{up} = \frac{P}{P_1}, \eta_c$ is the coupling efficiency of the sum-frequency radiation to the APD which can be close to 1, and η_{APD} is the conversion efficiency of the APD. For the strucutes considered earlier and the pump intensity $I_2 \sim 10^6$ W/cm^2, we obtain η in the $1-3\%$ interval. The efficiency is much higher for collinear in-plane propagation of the signal and pump beam. The overall responsivity defined as the ratio of the APD photocurrent to the mid-IR signal power P_1 incident on a crystal is given by

$$R = \frac{I_{APD}}{P_1} \tag{4.30}$$

$$= \eta_{up}\eta_c R_{APD}. \tag{4.31}$$

Where R_{APD} is the APD responsivity.

CHAPTER V

CONCLUSIONS

We considered sum frequency generation in an asymmetric double quantum well of GaAs/AlGaAs and InGaAs/AlInAs structures. We studied the intersubband nonlinear absorption of asymmetric double quantum wells designed for mid/far-infrared range. We also studied the dependance of second-order nonlinear susceptibility on various parameters of the well. We also observed that InGaAs/AlInAs has one advantage compared to GaAs/AlGaAs system: the electron effective mass in InGaAs is 35% smaller than in GaAs due to which for the same intersubband transition energies InGaAs has larger dipole matrix elements. However, the smallest linewidths measured by absorption spectroscopy have been found in the GaAs/AlGaAs system. We also studied figures of merit of the detector. The detectors using frequency up-conversion usually show high detectivity at the cost of low efficiency. In order to obtain high efficiency one needs to have large $\chi^{(2)}$ and long interaction or coherance length. With our detection scheme we have not only achieved high detectivity but also good quantum efficiency due to high nonlinearity. Our scheme is independent of temperature, i.e it is not sensitive to temperature as direct detection scheme. Single photon counting is also possible due to low noise, low dark currents and high detectivity. In conclusion, the proposed mid/far-IR photodetection scheme has the potential of reaching very high room temperature detectivity values comparable to that of state of the art near-IR APDs. There is a trade-off between the detectivity and photon conversion efficiency which originates from spontaneous emission by carriers generated in QWs by a strong pump. For the pump intensities supplied by a 100 mW semiconductor laser the conversion efficiency is of the order of a few percent. We can also achieve single photon detection based on the proposed geometry.

REFERENCES

[1] A. Rogalski, *Infrared Photo Detectors*, (SPIE Optical Engineering Press, Bellingham, Washington, 1995).

[2] B. Levine, J. Appl. Phys **74**, R1 (1993).

[3] H. C. Liu, C. Y. Song, Z. R. Wasilewski, A. Shen, M. Gao, and M. Bucchan., Appl. Phys. Lett **77**, 2437 (2000).

[4] H. Schneider, D. Luk, and H. C. Liu, *Quantum Well Infrared Photodetectors Physics and Applications*, (Springer, NewYork, 2007).

[5] G. Temporao, S. Tanzilli, T. Allen, M. Giovannini, H. Zbinden, N. Gisin, and J. Faist., Opt. Lett **31**, 1094 (2006).

[6] C. Langrock, E. Diamanti, Y. Yamamoto, H. Takesue, R. V. Roussev, and M. M. Fejer., Opt. Lett **30**, 1725 (2005).

[7] S. Tanzilli, L. Krainer, A. Rochas, I. Rech, S. Cova, H. Zbinden, N. Gisin, R. T. Thew, and S. C. Zeller., New J. Phys **8**, 32 (2006).

[8] A. Wojcik, F. Xie, V. Chaganti, Y. Cho, A. Belyanin, and J. Kono., J. Appl. Phys 'in press' (2008).

[9] E. Rosencher and B. Vinter, *Optoelectronics*, (Cambridge University Press, New York, 2002).

[10] J. B. Khurgin, *Nonlinear Optics in Semiconductors*, (Academic Press, San Diego, California, 1999).

[11] L. C. West and J. L. Eglash, Appl. Phys. Lett **46**, 1156 (1985).

[12] M. K. Gurnick and T. A. DeTemple, IEEE J. Quantum Electron **19**, 791 (1983).

[13] J. B. Khurgin, J. Opt. Soc. Am. **6**, 1673 (1989).

[14] A. Belyanin, F. Capasso, and M. Troccoli, *Intersubband Transitions in Quantum Structures*, (McGraw-Hill, Hightstown, New Jersey, 2006).

[15] C. Gmachl, O. Malis, and A. Belyanin, *Intersubband Transitions in Quantum Structures*, (McGraw-Hill, Hightstown, New Jersey, 2006).

[16] F. Capasso, F. Xie, A. Belyanin, M. Fischer, A. Wittmann, J. Faist, M. A. Belkin., Appl. Phys. Lett **92**, 201101 (2008).

[17] M. Belkin, F. Capasso, A. Belyanin, D. L. Sivco, A. Y. Cho, D. C. Oakley, C. J. Vineis, and G. W. Turner., Nature Photonics **1**, 288 (2007).

[18] M. Troccoli, A. Belyanin, F. Capasso, E. Cubukcu, D. L. Sivco, and A. Y. Cho., Nature **433**, 845 (2005).

[19] A. Wojcik, F. Xie, Y. Cho, V. Chaganti, A. Belyanin, and J. Kono., J. Modern. Opt 'in press' (2008).

[20] S. Pellegrini, R. E. Warburton, and J. J. Lionel, IEEE J. Quantum Electronics **42**, 397 (2006).

VITA

V. R. Chaganti received her Bachelor of Science degree in physics from the Sri Sathya Sai University at Ananthapur, India in 1999. She received her Master of Science degree in physics from University of Hyderabad, India in 2001. She entered physics program at Texas $A\&M$ University in September 2005 and graduated with her M.S. in December 2008. Mrs. Chaganti's email is chaganti@tamu.edu. Her contact address is Department of Physics, Texas $A\&M$ University, 4242 TAMU, College Station, TX 77843-4242.

The typist for this thesis was V. R. Chaganti.